Extreme ultraviolet carrier-frequency shearing interferometry of a lithographic four-mirror optical system

Patrick P. Naulleau[a] and Kenneth A. Goldberg
Center for X-Ray Optics, Lawrence Berkeley National Laboratory, Berkeley, California 94720

Jeffrey Bokor
Center for X-Ray Optics, Lawrence Berkeley National Laboratory, Berkeley, California 94720 and Electrical Engineering and Computer Science Department, University of California, Berkeley, California 94720

(Received 1 June 2000; accepted 2 August 2000)

The phase-shifting point diffraction interferometer (PS/PDI) has recently been developed to address the problem of at-wavelength metrology of extreme ultraviolet (EUV) optical systems. Although extremely accurate, the fact that the PS/PDI is limited to use with coherent EUV sources, such as undulator radiation, is a drawback for its widespread use. An alternative to the PS/PDI, with relaxed coherence requirements, is lateral shearing interferometry (LSI). Here we describe various LSI implementations and demonstrate the use of a cross-grating, carrier-frequency configuration to characterize a large-field 4×-reduction EUV lithography optic. The results obtained are directly compared with PS/PDI measurements. © *2000 American Vacuum Society.*
[S0734-211X(00)12806-9]

I. INTRODUCTION

The recent development of extreme ultraviolet (EUV) optics for use in next-generation lithography systems has led to several advancements in EUV interferometry.[1–4] With a demonstrated reference-wave front accuracy of better than $\lambda_{\mathrm{EUV}}/350$ (0.04 nm at $\lambda_{\mathrm{EUV}}=13.4\,\mathrm{nm}$),[5] the phase-shifting point diffraction interferometer (PS/PDI)[4–6] is, to the best of our knowledge, the highest accuracy EUV interferometer available. The PS/PDI has the drawback, however, of being limited to use with highly coherent EUV sources such as undulator radiation.[7]

An alternative to the PS/PDI, with relaxed coherence requirements, is the lateral shearing interferometer (LSI).[8–12] The Ronchi interferometer[8] is perhaps the simplest realization of the LSI. Although not yet fully characterized for accuracy at EUV, this type of interferometer has previously been used for at-wavelength characterization of EUV optics.[1–3] More recently, a cross-grating, carrier-frequency implementation of the Ronchi interferometer has been used in the characterization of an EUV Schwarzschild objective.[13] Direct comparison of this LSI to the PS/PDI has demonstrated a root mean square (rms) measurement agreement of $\sim\lambda_{\mathrm{EUV}}/71$.[13]

Here we describe the use of the cross-grating, carrier-frequency LSI for testing a lithographic four-mirror EUV optical system. The tests were performed in the same experimental chamber that houses the new EUV PS/PDI[14,15] designed to test commercial-scale large-field EUV optics. The LSI results are directly compared to PS/PDI measurements performed on the same optic. Furthermore, we propose an enhanced LSI configuration that overcomes some of the limitations of the carrier-frequency implementation used here.

[a]Electronic mail: pnaulleau@lbl.gov

II. CROSS-GRATING, CARRIER FREQUENCY LATERAL SHEARING INTERFEROMETER

In the LSI, the test wave front of interest is ideally compared to a single sheared version of itself rather than being compared to a well-defined reference, as is the case in the PS/PDI. The phase directly recovered from the recorded interferogram thus approximates the derivative of the underlying wave front in the direction of the shear. The underlying test-beam wave front can be recovered from the recorded wave front derivative through, for example, an integration process. To unambiguously reconstruct a wave front without rotational symmetry, two nonparallel derivative measurements are required.

When implementing a LSI at EUV it is convenient to use diffractive elements to produce the shear. Furthermore, for efficiency purposes, it is beneficial to limit the number of optical elements used. As first proposed by Ronchi,[8] one of the simplest LSIs meeting these criteria is a single transmission grating placed near the test-optic focus. When using a simple grating, performing two (typically orthogonal) derivative measurements requires rotating or replacing the grating between measurements. This could be particularly troublesome for high accuracy (better than $\lambda_{\mathrm{EUV}}/100$) EUV applications due to the tight tolerances required of the grating longitudinal plane coincidence (better than 0.1 μm). As known for many years, however, this problem can be overcome by using a cross grating[11,12] which provides the two orthogonal shears simultaneously.

Another complication with the simple grating implementation, especially when square-wave Ronchi rulings are used, is multiple- (more than two) beam interference causing confusion in the data analysis process. The multiple-beam interference problem has been addressed in various ways.[11,16–18] One solution is to use double-frequency gratings where only the first diffracted orders of the two constituent gratings

overlap.[11] This method, however, is not well suited to EUV interferometry due to the difficulty in fabricating the dual-high-frequency gratings. Achieving full order separation when testing an EUV optic ($\lambda = 13.4$ nm) with a moderate numerical aperture (NA) of 0.1 would require a grating pitch of 67 nm with accuracy to a small fraction of that pitch.

Another solution to the multiple-beam interference problem is ac heterodyning.[16] This method was used in earlier implementations of the EUV LSI.[1,3] In this case, the grating is translated laterally, orthogonal to the grating lines, producing temporal modulation of the intensity at each pixel at the detector. Temporal filtering is used to eliminate higher-order interference terms. Achieving high accuracy with this method when square-wave gratings are used, and hence square-wave temporal modulation is produced, requires a large number of samples to be recorded with very accurate grating translation. Because EUV systems are typically limited to using square-wave (binary) gratings due to fabrication issues, this method does not provide a time-efficient solution.

A third solution to the overlap problem is the single-sideband method[17] in which the grating is placed between the test optic and its focal plane and a focal-plane spatial filter is used. Assuming that the grating-induced beam separation in the image plane is large relative to the image size, the spatial filter can be used to directly eliminate all but two orders produced by the grating. The potential complication involved in aligning the focal-plane spatial filter to the beams, however, is a drawback of this method.

More recently, a variant of the single-sideband method, in which no physical spatial filter is used, has been implemented at EUV.[13] In this case a numerical spatial filter is used after detection of the fringe pattern. This method relies on the fact that the higher-order shear terms produce harmonics of the fundamental fringe frequency. Extracting the fundamental from the recorded square-wave fringe pattern using a digital spatial filter eliminates these higher-order shear terms. Unlike the original single-sideband method, the *digital-sideband* method cannot distinguish between the two first-order terms that interfere with the zero-order term. This means that the reconstructed wave front will actually be the average of two laterally displaced derivative measurements. Experiments have shown this to be of minimal concern when small shears are used and high-quality optics are tested.[13]

The interferograms produced with the digital-sideband method can be analyzed using standard static-fringe analysis techniques. Noting that the Fourier transform fringe analysis method[19] inherently involves a numerical band-pass filter, it is well suited to this process. The Fourier transform method does, however, require the spatial fringe modulation bandwidth to be much smaller than the fundamental carrier frequency. This places practical limits on the aberration magnitudes that can be accurately measured. In practice, this is of minimal concern for the high-quality optical systems of interest here.

The digital-sideband method is equally well implemented with cross gratings. In this case the recorded interferogram is analyzed twice using two different Fourier-domain filters to reconstruct the two orthogonal derivative wave fronts.

III. DUAL-DOMAIN IMPLEMENTATION

In practice, it is difficult to strictly meet the bandwidth criterion described above that requires the spatial fringe modulation bandwidth to be much smaller than the fundamental carrier frequency. Failure to meet this criterion causes light from adjacent orders to spill into the signal band of interest, corrupting the measurement. This problem has recently been addressed in the PS/PDI through the development of a dual-domain data collection and analysis technique.[20] The method relies on collecting a temporally modulated series of carrier-frequency interferograms. The method is essentially a three-tiered filtering system composed of low-pass spatial filtering the test-beam electric field, band-pass spatial filtering the individual interferogram irradiance frames of a phase-shifting series, and band pass temporal filtering the phase-shifting series as a whole. The first step is physical and is achieved by way of focal-plane windows, whereas the last two steps are implemented numerically. The dual-domain technique is a combination of the ac-heterodyne and single-sideband methods described above. This method exchanges speed for noise suppression characteristics. As with the original single-sideband method, the dual-domain technique eliminates ambiguities caused by both first-order terms interfering with the zero-order term.

The dual-domain method is best described in the Fourier domain. We assume the detector to be in the far field of the focal plane; thus, spatial frequencies at the detector are equivalent to lateral displacements in the focal plane: $f_x \approx x/(\lambda z)$, where f_x is spatial frequency in the detector plane, x is lateral displacement in the focal plane, z is the distance between the focal and detector planes, and λ is the illumination wavelength. In the dual-domain method, a spatial filter comprised of two windows centered, respectively, on two diffracted orders of the grating is placed in the focal plane. The window widths are chosen small enough to prevent spatial-frequency crosstalk between adjacent orders in the recorded interferogram. This differs from the original single-sideband method, which typically uses a single image-plane window to pass both orders.

Noting that the recorded interferogram is simply the modulus squared of the Fourier transform of the focal-plane field distribution, the autocorrelation theorem can be used to find the spatial-spectrum limits of the recorded interferogram. Figure 1(a) depicts the limits of the detector-plane-field spectral content in one dimension as set by the image-plane spatial filter (windows) and Fig. 1(b) shows the autocorrelation of the field spectrum or the recorded intensity spectrum. The central peak is the *zero-order* term: this is essentially the irradiance of the light passing through the windows. The two off-axis components are the positive- and negative-first-order terms that arise from the interference between the sheared beams. To prevent overlap between adjacent orders, the window separation, and hence focal-plane beam separation, is required to be at least twice the window

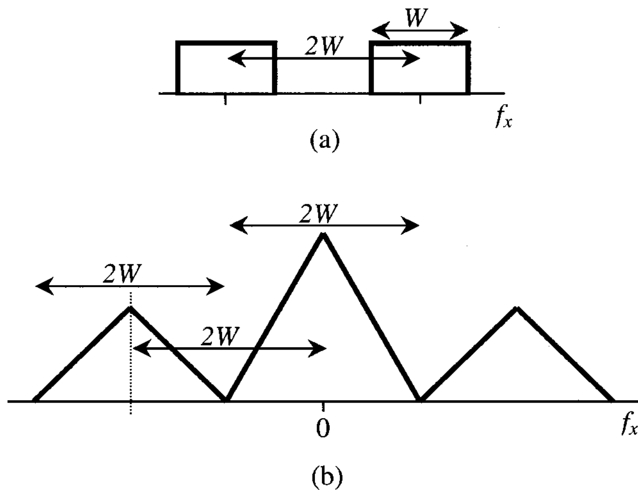

FIG. 1. (a) Limits of the detector-plane-field spectral content in one dimension as set by the image-plane spatial filter. (b) Spatial-spectrum limits of the recorded interferogram. By way of the autocorrelation theorem this is the autocorrelation of the detector-plane field spectrum.

width. This separation differs from the PS/PDI dual-domain case in which the beam separation is only required to be 3/2 the window width.[20] The difference comes from the fact that in the PS/PDI the reference-beam spectrum is essentially a delta function, whereas in the LSI, the reference is a copy of the test beam.

Another advantage of the dual-domain method is that by physically filtering in the focal plane, limitations imposed by the Talbot effect[21] are eliminated. The Talbot effect restricts the selection of the grating longitudinal position to a discrete set of planes; this in turn limits the choice of the spatial-carrier frequency in the recorded interferogram. We note that this advantage is also achieved using the above mentioned single-sideband method. As with the single-sideband method, however, the dual-domain method involves a more complicated alignment procedure than does the digital-sideband method.

IV. EXPERIMENTAL RESULTS

The digital-sideband LSI described above has been implemented at EUV to characterize a lithographic four-mirror EUV optical system operating at a wavelength of 13.4 nm and a NA of 0.1 providing approximately 100 nm resolution.[22] The interferometry was performed using an undulator beamline[7] at the Advanced Light Source synchrotron radiation facility at Lawrence Berkeley National Laboratory. Due to the coherence properties of the undulator beamline light,[7] the LSI has been demonstrated with coherent illumination. The spherical nature of the illumination is guaranteed by way of a ~250 nm pinhole spatial filter placed in the object plane (the same configuration as used for the PS/PDI).[15] The tests were performed at the optic operational wavelength of 13.4 nm with a spectral resolution, $\lambda/\Delta\lambda$, of approximately 350.

The LSI wave front measurements were compared to PS/PDI results obtained from the same optic in the same experimental chamber. Figure 2 shows the configurations for both the LSI and the PS/PDI; only minor modifications are required to switch between configurations. The cross-grating implementation was chosen, allowing the two orthogonal shear measurements to be obtained in parallel. A 2 μm pitch grating was placed approximately 300 μm from focus, yielding about 30 fringes over the NA of the optic. This configuration provides a shear of approximately 1/15 the NA.

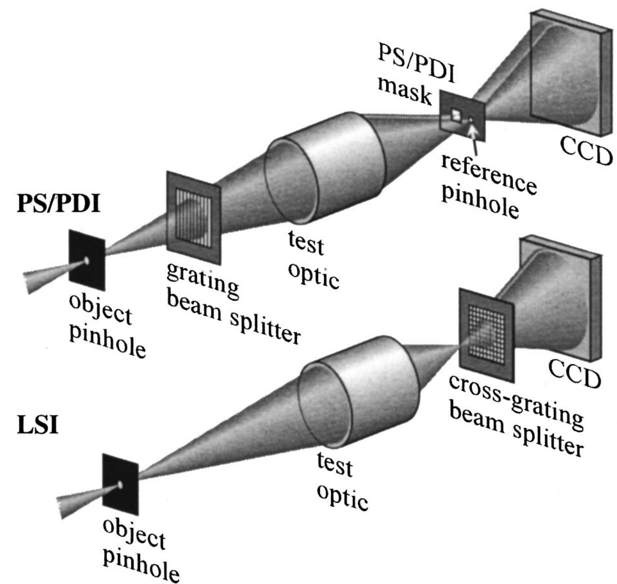

FIG. 2. Experimental configurations for both the PS/PDI and the LSI. Only minor modifications are required to switch from one configuration to the other. The LSI uses a single cross grating placed slightly out of the focal plane, allowing the two orthogonal shear terms to be measured simultaneously.

The test optic is a 4×-demagnification ring-field system with a 26 mm image-side chord length[22] and was characterized at 35 field points spanning the field of view. The measurement points were defined by an array of pinholes in the object plane and a corresponding array of gratings near the image plane. The individual points were interrogated by moving the entire interferometer under the stationary undulator beam focused to a sub-10 μm spot in the object plane.

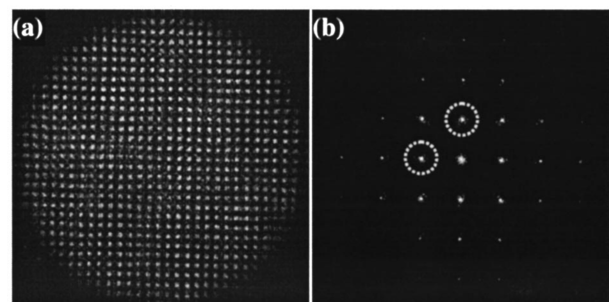

FIG. 3. (a) Representative LSI interferogram with the cross grating placed approximately 300 μm from focus and (b) its Fourier transform revealing the isolated, orthogonal interference terms, along with the higher-order terms. The dashed outlines indicate the approximate positions of the Fourier-domain filters used in the phase recovery process.

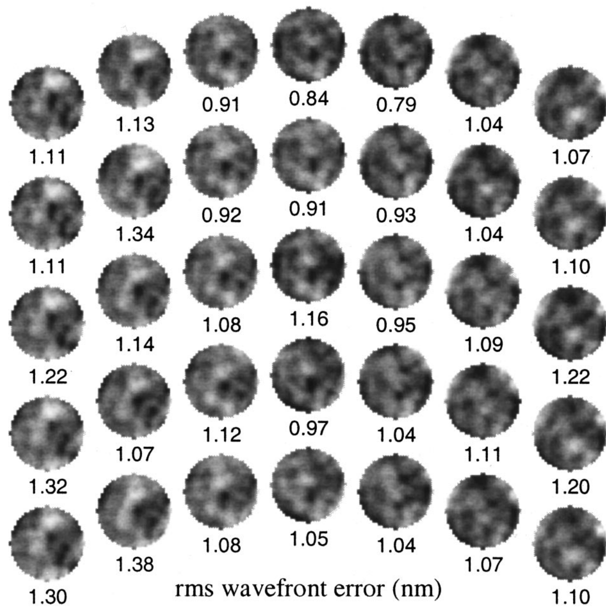

FIG. 4. Reconstructed wave fronts at each of the 35 measured field points over a NA of 0.091. The rms wave front error magnitude, as measured from a 37-term Zernike polynomial decomposition, varies from 0.79 to 1.38 nm across the field.

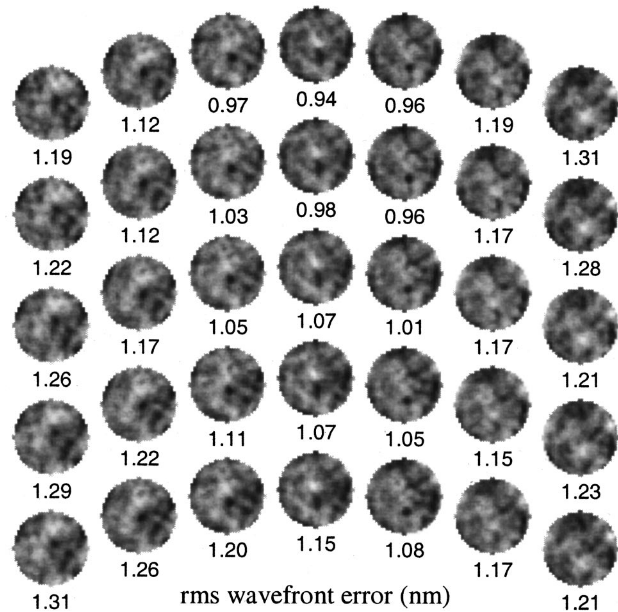

FIG. 5. PS/PDI data from Ref. 15 reanalyzed over the same grid size (30×30) and NA (0.091) as used for the LSI measurements presented here. The rms wave front error magnitude is measured from a 37-term Zernike polynomial decomposition.

Figure 3 shows a representative interferogram and its Fourier transform, revealing the isolated orthogonal interference terms along with the higher-order terms. To extract the two orthogonal derivative wave fronts, the interferogram is analyzed twice using the Fourier transform method.[19] The analysis uses two orthogonally displaced Fourier-domain filters. The approximate positions of the filters are indicated by the dashed outlines in Fig. 3(b). The wave fronts reconstructed by the Fourier transform method are combined to recover the underlying test-beam wave front using the Rimmer method.[23] To avoid artifacts caused by the transition from the three-beam to two-beam interference areas, the wave front reconstruction is limited to the three-beam interference area (0 and ±1 orders), leading to a slightly reduced measurement NA. The NA of the measurements presented here is 0.091 instead of the full 0.1. This limitation would be avoided by using the original single-sideband or dual-domain methods described above.

Figure 4 shows the resulting wave fronts at the 35 measured field points. The rms wave front error, as measured from a 37-term Zernike polynomial decomposition, is seen to vary from 0.79 to 1.38 nm across the field of view. The 1/15 NA shear causes the spatial sampling of the reconstructed wave fronts to be limited to a full width of 30 pixels.[23]

The PS/PDI-measured wave fronts at these same field points (over a larger NA) are presented elsewhere.[15] For direct comparison to LSI, Fig. 5 shows the PS/PDI data reanalyzed over the same grid size (30×30) and NA (0.091) as used for the LSI. Good qualitative agreement is evident. Although identical filtering was used in determining the constituent wave fronts, the PS/PDI data show more spatial frequency content; this is due to the averaging induced by three-beam interference effect (described above) present in the digital-sideband method. This effect could be minimized by reducing the shear, or altogether eliminated by using the dual-domain or single-sideband methods.

The quantitative agreement between LSI and PS/PDI is determined by performing a point-by-point subtraction of the LSI and PS/PDI wave fronts at each field point and taking the rms magnitude (as measured from a 37-term Zernike polynomial decomposition) of the resulting difference wave front as the agreement. Figure 6 shows the agreement as a function of field point. The average agreement between the two measurements is 0.037 waves (0.49 nm or $\lambda_{\mathrm{EUV}}/27$)

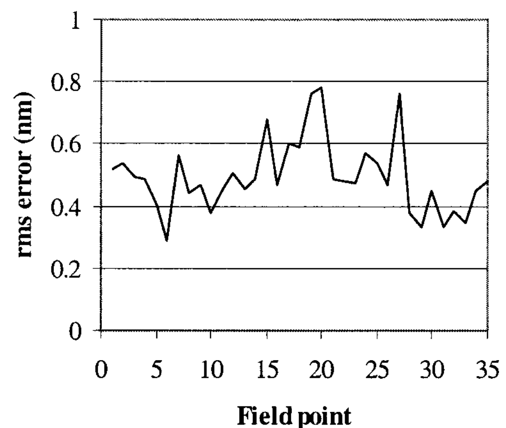

FIG. 6. Plot of the rms agreement between separate LSI and PS/PDI measurements at each field point. The rms agreement is determined by reanalyzing the PS/PDI data in Ref. 15 over the same grid size and NA as used for the LSI measurements presented here and performing a point-by-point subtraction of the wave fronts at each field point. The rms magnitude as measured from a 37-term Zernike polynomial decomposition of the resulting difference wave front is taken as the agreement.

with a standard deviation of 0.009 waves. We note that in a previous comparison, an agreement of $\lambda_{EUV}/71$ (Ref. 13) had been found. The discrepancy is most likely due to the fact that more averaging was performed in the earlier case; a total of 30 LSI measurements was averaged, whereas for the data presented here only 5 LSI measurements were averaged at each field point. Also, the NA in the earlier measurement was approximately 10% smaller than the NA considered here.

Although good agreement has been demonstrated between the EUV PS/PDI and the digital-sideband implementation of the EUV LSI, it is important to note that, due to the constraints of our undulator beamline, this was accomplished with coherent illumination. The primary benefit of the LSI, however, is its ability to operate under broad-source illumination.[3] Modification of our beamline to allow direct comparisons between the PS/PDI and a broad-source implementation of the LSI is presently under investigation.

ACKNOWLEDGMENTS

The authors are greatly indebted to Erik Anderson for nanofabrication, Phil Batson for engineering support, and the entire CXRO staff for enabling this research. Special thanks are due to Paul Denham for expert help with experimental systems. They also acknowledge valuable discussions with Avi Ray-Chaudhuri and John Bjorkholm. This research was supported by the Extreme Ultraviolet Limited Liability Company, the Semiconductor Research Corporation, DARPA Advanced Lithography Program, and the DOE Office of Basic Energy Science.

[1] J. E. Bjorkholm, A. A. MacDowell, O. R. Wood II, Z. Tan, B. LaFontaine, and D. M. Tennant, J. Vac. Sci. Technol. B **13**, 2919 (1995).
[2] A. K. Ray-Chaudhuri, W. Ng, F. Cerrina, Z. Tan, J. Bjorkholm, D. Tennant, and S. J. Spector, J. Vac. Sci. Technol. B **13**, 3089 (1995).
[3] A. K. Ray-Chaudhuri, K. D. Krenz, and C. H. Fields, J. Vac. Sci. Technol. B **15**, 2462 (1997).
[4] H. Medecki, E. Tejnil, K. A. Goldberg, and J. Bokor, Opt. Lett. **21**, 1526 (1996).
[5] P. Naulleau, K. Goldberg, S. Lee, C. Chang, D. Attwood, and J. Bokor, Appl. Opt. **38**, 7252 (1999).
[6] K. A. Goldberg, Ph.D. dissertation, University of California, Berkeley, 1997.
[7] D. Attwood *et al.*, IEEE J. Quantum Electron. **35**, 709 (1999).
[8] V. Ronchi, Appl. Opt. **3**, 437 (1964).
[9] A. Lohmann and O. Bryngdahl, Appl. Opt. **6**, 1934 (1967).
[10] S. Yokozeki and T. Suzuki, Appl. Opt. **10**, 1575 (1971).
[11] J. C. Wyant, Appl. Opt. **12**, 2057 (1973).
[12] H. O. Bartlelt and Y. Li, Opt. Commun. **48**, 1 (1983).
[13] K. A. Goldberg, P. Naulleau, and J. Bokor, Appl. Opt. (submitted).
[14] K. A. Goldberg, P. Naulleau, P. Batson, P. Denham, H. Chapman, and J. Bokor, Proc. SPIE **3997**, 867 (2000).
[15] K. A. Goldberg, P. Naulleau, P. Batson, P. Denham, E. Anderson, H. Chapman, and J. Bokor, J. Vac. Sci. Technol. B, these proceedings.
[16] J. C. Wyant, Appl. Opt. **14**, 2622 (1975).
[17] J. Schwider, Appl. Opt. **20**, 2635 (1981).
[18] J. Braat and A. Janssen, J. Opt. Soc. Am. A **16**, 131 (1999).
[19] M. Takeda, H. Ina, and S. Kobayashi, J. Opt. Soc. Am. **72**, 156 (1982).
[20] P. Naulleau and K. A. Goldberg, Appl. Opt. **38**, 3523 (1999).
[21] D. Malacara, *Optical Shop Testing* (Wiley, New York, 1992), pp. 346–347.
[22] D. W. Sweeney, R. Hudyma, H. N. Chapman, and D. Shafer, Proc. SPIE **3331**, 2 (1998).
[23] M. P. Rimmer, Appl. Opt. **13**, 623 (1974).